Optical Characterization of Ultrasmall Si Nanoparticles Prepared through Electrochemical Dispersion of Bulk Si

Dean A. Eckhoff,* Jason D. B. Sutin, Robert M. Clegg, and Enrico Gratton

Department of Physics and Laboratory for Fluorescence Dynamics, University of Illinois at Urbana-Champaign, 1110 West Green Street, Urbana, Illinois 61801

Elena V. Rogozhina and Paul V. Braun

Department of Materials Science, Beckman Institute, and Materials Research Laboratory, University of Illinois at Urbana-Champaign, 1304 West Green Street, Urbana, Illinois 61801

Received: April 28, 2005; In Final Form: July 6, 2005

Studying the properties and stability of silicon nanoparticles (Si-np) in aqueous environments may lead to novel applications in biological systems. In this work, we use absorption and photoluminescence (PL) spectroscopy to characterize ultrasmall Si-np prepared through anodic etching and ultrasonic fractionation of a crystalline Si wafer. Their behavior is studied over time in 2-propanol and during treatments with water, NaOH, HCl, and H_2O_2. The observed population is divided into two types of material: bright species consisting of well-etched Si-np, ∼1 nm in diameter, and dark species derived from partially etched or aggregated Si structures. The dark material is seen by its scattering in the 2-propanol and water solutions and is largely removed via precipitation with the NaOH or HCl treatment. The bright material includes three distinct species with their respective emissions in the UV−B, UV−A, and hard-blue regions of the spectrum. The hard-blue PL is shown to have a simple pH dependence with a pK_a ∼3, providing an important insight into its chemical origin and signaling for possible application of Si-np as environmental probes. Our results offer some potential for tailoring the PL properties of ultrasmall Si-np through control of their surface chemistry.

I. Introduction

Luminescent semiconductor nanoparticles offer a challenging opportunity to explore the photophysics and chemistry of materials in the intermediate regime between bulk and molecular behavior. Among their many unique optical and electronic properties is the ability to emit efficient, size-tunable photoluminescence (PL) in the visible and near-visible regions of the spectrum. Recently, the group IV semiconductor Si, and to a lesser extent Ge, has received considerable interest[1−25] with researchers working toward applications in the wide ranging areas of fluorescent lighting, optoelectronics, and as luminescent markers for biophysical systems. Here, we report on the optical characterization of ultrasmall silicon nanoparticles (Si-np), ∼1 nm in diameter and with strong PL in the near-UV to blue. The emphasis is on their behavior in aqueous environments and their potential applications as solution-phase, luminescent markers for biological systems.

Most of the investigations in this area have focused on the direct gap, compound quantum dots (CQDs) such as ZnS, CdSe, GaAs, and InP nanoparticles.[26−35] Progress with the core−shell synthesis approach[26] has led to the development of luminescent materials with narrow and tunable emission,[27−29] excellent photostability,[28−31] and a brightness approaching the theoretical limit for a given size.[32] For biological applications, however, it is necessary to add another layer of material: a coat of hydrophilic, bifunctional linkers that help to mask the toxicity of the core−shell CQD and provide stability in aqueous environments.[27−28,31,33] The resulting core−shell−coat CQD (e.g., CdSe−ZnS−silane) can then be further functionalized for uses such as protein labeling[31,34−35] and cellular imaging.[29−32]

The multilayered approach to nanoparticle preparation, required for stabilization of CQDs, has two important characteristics that limit the range of possible applications. First is the relatively large size of the final product, which is currently on the order of 10−15 nm and has a practical minimum of at least 3−5 nm. This excludes many possible applications studying small to mid-size biomolecules, where the additional mass and volume of the CQD would be a major perturbation to the system. The second characteristic is that the PL originating from the semiconductor core has been largely decoupled from the environment. While this has many inherent benefits, it also limits their utility as a direct probe of the local surroundings, with CQDs generally serving rather as an inactive or passive marker.

To address these limitations, the group IV semiconductors Si and Ge are a promising alternative. The same type of core−shell and core−shell−coat motifs are available to this class of material (e.g., Ge−SiO_2−silane).[1,2] In addition, given the lower inherent toxicity of silicon,[36] along with the extensive literature on its surface and molecular chemistries (e.g., see refs 37−39), it seems likely that some of the steps required for CQD stabilization may be reduced or eliminated altogether for Si-np, generally yielding smaller overall sizes. They also have the advantage of direct compatibility with organic materials via the strong and stable Si-C bond, providing a larger degree of freedom and flexibility in possible surface passivations and functionalities.[3−7,40−43] For example, it was recently demonstrated that H-passivated Si-np can be directly functionalized through a Si−C linkage terminating with a carboxylic acid group toward the solvent. This modification preserves the strong PL of the Si core, adds a hydrophilic interface for stability in aqueous media, and is easily reacted with primary amines to

* Corresponding author: E-mail: deckhoff@uiuc.edu.

10.1021/jp052214e CCC: $30.25
Published on Web 10/01/2005

label biomolecules, all while adding only a small amount to the overall size.[7]

Work with the Si and Ge systems has also shown that surface chemistry can play a more direct role in their photophysical behavior. The analysis has generally focused on the source of PL and the debate between the quantum confinement (delocalized) and surface state (localized) mechanisms. Researchers studying porous Si structures,[40−57] for example, have attributed the PL to various sources ranging from quantum-confined nanorods and nanodots[44−46] to surface state silanone and siloxane groups.[47−56] For Si and Ge nanoparticles prepared through various routes such as solution-phase synthesis,[1−4,8−9] electrochemical etching,[10−13] laser ablation,[14,15] and using supercritical fluids,[16−18] the suggested PL sources have ranged from delocalized quantum confinement states[15] to localized Si−Si surface dimer states.[19−21] This apparent range of available mechanisms is seen more clearly in recent computational modeling of nanoscale Si and Ge clusters, which has shown transitions ranging from delocalized core states in H-passivated Si-np to localized surface states for particles containing a silanone (Si═O) group.[22−25]

These prospects raise the exciting potential for controlling the PL properties of Si and Ge nanoparticles by using different treatments to create the desired surface chemistry. In this contribution, we explore the aggregation and PL behavior of ultrasmall (∼1 nm) Si-np prepared through electrochemical dispersion of bulk Si. The samples are studied over time in 2-propanol and during treatments with water, NaOH, HCl, and H_2O_2. The PL displays three distinct, near-Gaussian states with their respective emissions in the UV−B (∼305 nm), UV−A (∼340 nm), and hard-blue (∼400 nm) regions of the spectrum. The hard-blue emission is shown to have a strong pH dependence with a pK_a ∼3, demonstrating the potential for using Si-np as environmental sensors. Based on a simplified model of surface oxidation, each of the three main states is correlated with a possible chemical origin including siloxane (Si−O−Si) and silanone (Si═O) based structures. Also detailed is the presence of dark material in the Si-np preparation, as seen with its aggregation and scattering in the 2-propanol and water solutions. After discussing some possible sources, it will be shown that the dark species are unstable and precipitate with the NaOH or HCl treatment, allowing for their separation from the bright material.

II. Experimental Section

A. Absorption and PL Spectra. Transmission spectra were measured on a Perkin-Elmer (Boston, MA) UV−vis spectrophotometer using a quartz cuvette with 1 cm path length. The measured OD was corrected for solvent−cuvette background. Photoluminescence spectra were measured on a Jobin Yvon (Edison, NJ) FluoroMax-2 fluorimeter with the same samples and conditions used for the transmission spectra. The signals were corrected for instrument response and lamp power. All of the compounds used (2-propanol, water, HCl, NaOH, and H_2O_2) were checked for background with identical transmission and PL measurements. The 2-propanol was the only one of these with detectable impurities. Its absorption cutoff (A > 1.0 cm^{-1}) was 205 nm and trace PL, minor compared to the Si-np PL, was excitable ∼250−300 nm.

The measured OD spectra (Figures 1−4) are modeled as the sum of a $1/\lambda^n$ scattering component, fit to the visible region from 400 to 700 nm, and a Gaussian absorber, fit to match the UV shoulder ∼240−300 nm. A typical example of the decomposition into scattering and absorbing components is shown in Figure 1 for the fresh Si-np in 2-propanol. The parameters for the fits (the scattering amplitude and exponent and the absorption wavelength, amplitude, and width) were obtained using a least-squares minimization. The results are summarized in Table 1 and will be used to help illustrate overall trends among the various samples studied. For these measurements, the region below ∼240−250 nm was not explored reliably. Generally, the absorption rises very quickly below this limit, and for the concentrations studied, the values were beyond the instrument response (A ∼2−3). In some cases, this quick rise in absorption skewed the blue-edge of the Gaussian component and the fits were made with only the back half to two-thirds of the absorption shoulder.

One of the tools used in the modeling and presentation of the PL data is the white-light emission spectrum (WES). The WES is equivalent to the emission expected for "white-light excitation" with a band of wavelengths from λ_{min} to λ_{max}. It is calculated as the sum of PL intensities over a range of excitation wavelengths:

$$\mathrm{WES}(\lambda_{em}) = \int_{\lambda min}^{\lambda max} I(\lambda_{ex},\lambda_{em})\cdot \mathrm{d}\lambda_{ex}$$

where the subscripts 'ex' and 'em' refer to the excitation and emission wavelengths, respectively. We have chosen to use the WES because it captures all of the significant emissions, regardless of excitation, within a single spectrum. This makes it useful for studying the ensemble behavior of heterogeneous systems and helping to illustrate the overall trends among many different samples. Since the integration may average over some of the details, all conclusions drawn from the WES were checked for consistency with the individual PL spectra.

For this work, the WES is calculated using excitation wavelengths from 250 to 400 nm (10 nm increments) and collecting emissions up to 550 nm. The lower bound of 250 nm is near the blue-edge of the excitation peaks (Figures 5, 9, and 10) and absorption peaks (Figures 1−4, shoulder ∼240−300 nm). For the upper bounds, no significant PL was seen for excitations greater than 340 nm or emissions greater than 500 nm.

The PL data is analyzed by modeling the WES (see Figures 2−4 and 7) as a sum of Gaussian components. The modeling is intended only as a rough fit to help see overall trends in the spectral behavior (e.g., significant red-shifts). A near-Gaussian line shape for the emissions with a fwhm ∼0.4 to 0.5 eV is seen in the individual PL spectra shown in Figures 1, 5, 6, 9, and 10. Table 2 summarizes the fit parameters for the seven samples (fourteen measurements) that are discussed in this report. The WES was fit to four components, which was sufficient to cover all of the emissions from 260 to 550 nm. The four components had peak wavelengths in the UV−B (300−309 nm), UV−A (336−352 nm), hard-blue (380−401 nm), and blue (450−466 nm) regions of the spectrum. It is not our intent to suggest that in all cases these spectral components correspond to individual chemical species. In the discussion section, we will attempt to be clear on this point by highlighting the instances when a given component appears to be a distinct PL state (see IV-D, E, F), as well as the cases in which the distinctness is not so clear (see IV-G).

B. Si-np Preparation. The silicon nanoparticles (Si-np) were prepared with a H-passivation using previously described techniques.[10−13,57] In brief, a crystalline Si wafer is anodized with H_2O_2 and HF in a methanol/water bath to etch a porous surface layer. After a short wash to remove residual chemicals, the Si-np weakly embedded in the porous matrix (see also IV-

TABLE 1: Absorption Fit Parameters

		$1/\lambda^n$ scatterer		Gaussian absorber		
data set	sample (solvent)[a]	OD 400 nm (1/cm)	exponent, n	magnitude (1/cm)	peak WL (nm)	fwhm (eV)
Si-np, as-prepared	(a) Si-np stock (iso)	0.053	3.60	0.120	272	0.72
NaOH/HCl dilutions, fresh samples	(b) Si-np stock (iso)	0.012	2.92	0.029	267	0.73
	(c) Water dilution (wat)	0.026	3.07	0.028	269	0.68
	(d) NaOH dilution (wat)	0.005	3.74	0.031	266	0.93
	(e) HCl dilution (wat)	0.142	2.00	0.026	276	0.68
NaOH/HCl dilutions, aged four months	(f) Si-np stock (iso)	0.014	3.07	0.044	266	0.59
	(g) Water dilution (wat)	0.018	2.68	0.020	270	0.55
	(h) NaOH dilution (wat)	0.006	2.09	0.034	271	0.80
	(i) HCl dilution (wat)	0.005	2.70	0.023	273	0.61
HCl treatment, aged four months	(j) Si-np stock (iso)	0.038	3.10	0.074	264	0.59
	(k) HCl treated (iso)	0.001	4.00	0.014	271	0.62
H_2O_2 treatment, fresh samples	(l) Si-np stock (iso)	0.012	3.52	0.023	272	0.62
	(m) H_2O_2 dilution (wat)	0.017	3.52	*b*	*b*	*b*
	(n) H_2O_2 activated (wat)	0.005	3.03	*b*	*b*	*b*

[a] Solvent: iso = 2-propanol, wat = 3:1 water:2-propanol. [b] Spectrum skewed by H_2O_2 interference.

TABLE 2: Photoluminescence Fit Parameters

		fraction of total intensity (peak wavelength − nm)				total intensity,
data set	sample (solvent)[a]	UV−B em[b]	UV−A em[b]	hard-blue em[b]	blue em[c]	A.U.
Si-np, as-prepared	(a) Si-np stock (iso)	69% (309)	20% (344)	7.4% (385)	3.1% (457)	1.00
NaOH/HCl dilutions, fresh samples	(b) Si-np stock (iso)	68% (307)	21% (339)	8.3% (380)	2.9% (457)	1.00
	(c) Water dilution (wat)	51% (308)	30% (340)	14% (380)	5.3% (459)	1.20
	(d) NaOH dilution (wat)	24% (305)	55% (338)	16% (380)	4.3% (451)	1.31
	(e) HCl dilution (wat)	50% (309)	31% (343)	15% (381)	4.2% (456)	1.09
NaOH/HCl dilutions, aged four months	(f) Si-np stock (iso)	67% (304)[d]	20% (336)	8.0% (380)	5.5% (454)	1.59
	(g) Water dilution (wat)	41% (309)	33% (343)	19% (383)	6.4% (457)	0.82
	(h) NaOH dilution (wat)	12% (300)[e]	64% (338)[f]	18% (380)	6.5% (450)	0.68
	(i) HCl dilution (wat)	45% (304)[g]	31% (340)	18% (380)	6.5% (456)	0.27
HCl treatment, four months old	(j) Si-np stock (iso)	72% (307)[h]	18% (340)	7.8% (380)	2.5% (456)	1.00
	(k) HCl treated (iso)	59% (305)	15% (335)	23% (401)	2.5% (466)	0.15
H_2O_2 treatment, fresh samples	(l) Si-np stock (iso)	69% (309)	20% (342)	7.9% (383)	2.8% (453)	1.00
	(m) H_2O_2 dilution (wat)	49% (309)	29% (339)	15% (381)	7.4% (455)	1.05
	(n) H_2O_2 activated (wat)	35% (309)	32% (352)	24% (399)	9.4% (459)	0.96

[a] Solvent: iso = 2-propanol, wat = 3:1 water:2-propanol. [b] Unless otherwise specified, fwhm = 0.47 eV for the UV−B, UV−A, and hard-blue emissions. [c] fwhm ranged from 0.47 to 0.65 eV for the blue emission. [d−h] fwhm. [d] 0.54 eV. [e] 0.36 eV. [f] 0.40 eV. [g] 0.42 eV. [h] 0.51 eV.

A) are extracted via ultrasonic fractionation directly into the working solvent, spectroscopic grade 2-propanol. The addition of H_2O_2 to the etching bath, along with the use of a high current density during anodization, enhances the etching to yield finer features and tends to produce Si-np passivated with the monohydride surface species (≡SiH).[10−11,57] Previous analysis including high-resolution TEM imaging, size exclusion chromatography, and computational modeling shows that a discrete set of particle sizes is favored for the Si clusters etched from the wafer, the smallest of which is ∼1 nm in diameter.[10−11,21] For the conditions used here, the analysis suggests (see also IV-D) structures similar to the $Si_{29}H_{24}$ cluster (monohydride, ∼1 nm, Figure 11) as the dominant source of PL in the starting material. The absorption and PL spectra for the Si-np, freshly prepared in 2-propanol (sample a), are shown in Figure 1 and outlined in Tables 1a and 2a.

C. NaOH/HCl Dilutions. Four samples and eight measurements are included in this data set, as outlined in Tables 1 and 2. Measurements (b−e) are the freshly prepared dilutions (Figure 2) and measurements (f−i) are the same samples after four months aging in the dark (Figure 3). Each sample is a one-part dilution of stock Si-np in 2-propanol with three-parts of: (b, f) 2-propanol, (c, g) water, (d, h) NaOH, pH 11.6, and (e, i) HCl, pH 2.2. After mixing, all four samples were sonicated in steps for ∼90 min total and then visually inspected under white light illumination using a Dolan-Jenner Industries (Woburn, MA)

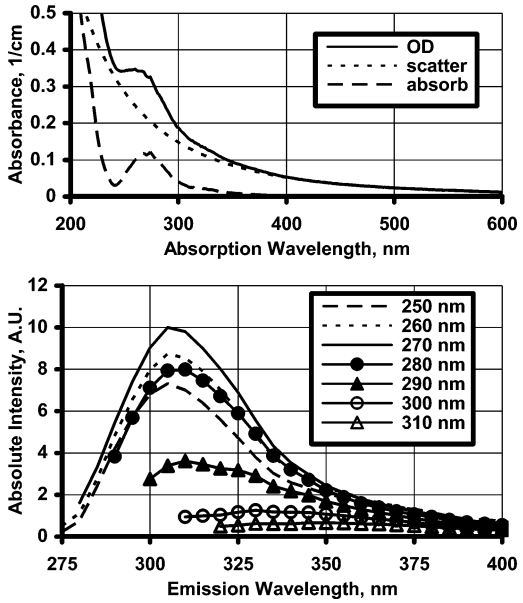

Figure 1. Si-np in 2-propanol, freshly prepared (sample a). (Top) Absorption spectra; total OD (solid) decomposed into scattering (short dash) and absorbing (long dash) components. (Bottom) PL emission spectra for excitations from 250 to 310 nm.

Fiber-Lite model 190 fiber optic lamp. The samples were then centrifuged to extract any solids and their absorption and PL

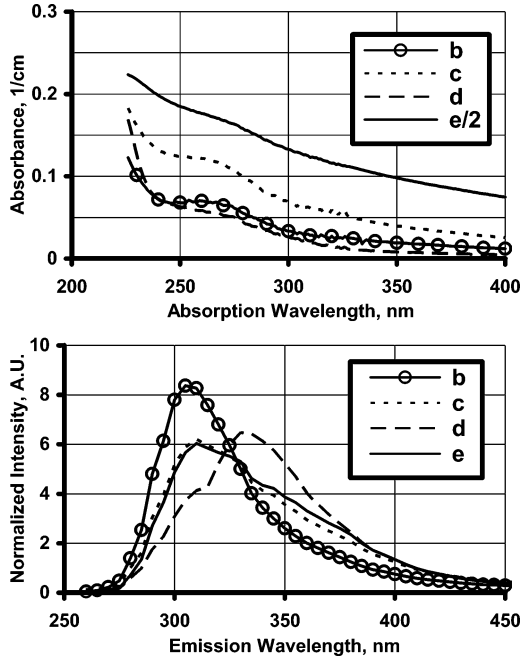

Figure 2. NaOH/HCl dilutions, freshly prepared (samples b−e). Each is one part Si-np in 2-propanol with 3 parts of: (b) 2-propanol, (c) water, (d) NaOH, and (e) HCl. (Top) Total OD (absorption + scattering). The absorbance of sample (e) is divided by two. (Bottom) White-light emission spectra.

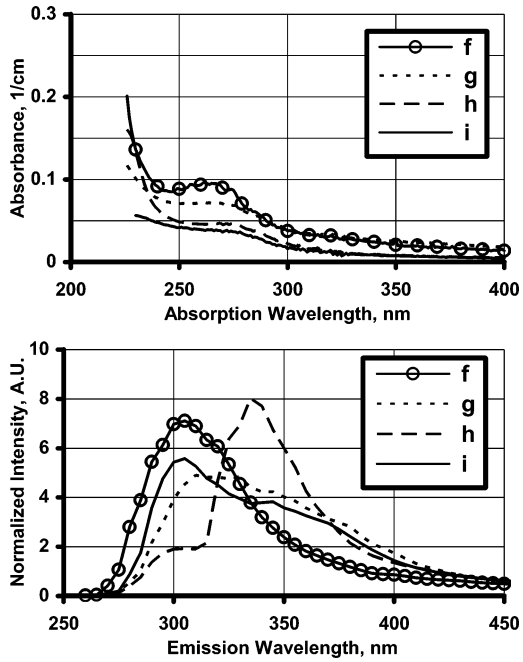

Figure 3. NaOH/HCl dilutions, aged four months (samples f−i). Each is one part Si-np in 2-propanol with 3 parts of: (f) 2-propanol, (g) water, (h) NaOH, and (i) HCl. (Top) Total OD (absorption + scattering). (Bottom) White-light emission spectra.

spectra were measured (Figure 2b−e). After four months aging in the dark, the same steps were repeated (Figure 3f−i).

D. HCl Treatment. Treatment with HCl was done by first removing the 2-propanol from a sample of stock Si-np (already aged four months) under vacuum with no heating. The solids were redispersed in aqueous HCl, pH 1.6, sonicated in steps for ∼2 h total, and allowed to rest for 24 h. Spectral measurements were then made at each step during a pH titration using small additions of NaOH. When the sample was neutralized, the water was removed under vacuum with no heating. Clean 2-propanol was added to the sample and, after sonication for ∼30 min, the undissolved material, including a large amount of NaCl, was removed via centrifugation. Figure 4 and Tables 1 and 2 show the absorption and PL spectra for two samples, both in 2-propanol: (j) the stock Si-np before treatment, already aged 4 months, and (k) the same material after the HCl treatment. Individual excitation and emission spectra are compared in Figures 5, 9, and 10, and spectral measurements during the pH titration are shown in Figure 6.

E. H_2O_2 Treatment. Treatment with H_2O_2 was done by first mixing one-part of the Si-np stock in 2-propanol with three-parts of aqueous H_2O_2 (0.1%). After 1 h, the absorption and PL spectra were measured, showing no significant activation of the peroxide; the PL spectra were nearly identical to a blank water dilution (Table 2c, m). The H_2O_2 was then activated by irradiating the sample with UV light at 250 nm for 30 min (incident power ca. 10 μW). After irradiation, the absorption spectrum showed clear activation of the peroxide and large changes in PL were observed. Control experiments with no H_2O_2 present show that most of the changes are attributable to free radical reactions and not direct irradiation of the Si-np (data not shown). For comparison, Figure 7 and Tables 1 and 2 show three samples for the H_2O_2 treatment: (l) the starting sample of Si-np in 2-propanol, (m) the sample diluted 4× in aqueous H_2O_2, and (n) the same sample after activation of the H_2O_2. Note that the intensities for measurement (l) are divided by four to account for the subsequent dilution. Also, the absorption spectra for measurements (m) and (n) are not included as they were skewed by the H_2O_2 absorption. Individual PL spectra for sample (n) are shown in Figure 8.

III. Results

A. Stock Si-np. The stock Si nanoparticles (Si-np) will serve as a basis for analyzing the different treatments studied in this work. Figure 1 shows the absorption spectrum and some emission spectra for the Si-np freshly prepared in 2-propanol (sample a). The absorption spectrum has a strong shoulder ∼240−300 nm overlapping with the peak excitation wavelengths. There is a strong tail in the absorption toward the red (λ > 300 nm), which is likely due to scattering, consistent with the faint cloudiness of the sample. Modeling of the data recovers a "true absorption" component with a peak ∼270 nm, as shown by the scatter-corrected spectrum included in Figure 1.

The PL shows a peak emission of 305 nm (4.1 eV) and a peak excitation of 270 nm (4.6 eV), giving a Stokes shift (peak-to-peak) of ∼0.45 eV. The overlap of the absorption and PL excitation peaks shows that the absorption feature is due, at least in part, to bright species. The peak emission wavelength is roughly constant (within ∼5 nm), and the intensity drops markedly for excitations greater than 290 nm. The line shape is near-Gaussian with a red-tail from ∼335 nm up into the blue. Modeling of the WES (Table 2a), calculated as the sum of the emission spectra in Figure 1, shows that the dominant emission in the freshly prepared Si-np is the UV−B state, which covers 69% of the total emission. Significant contributions are also seen from the UV−A and hard-blue emissions with relative strengths of 20% and 7.4% of the total, respectively. However, note that these minor emissions have poorly defined peaks.

B. NaOH/HCl Dilutions. Four samples and eight measurements are included in this data set, as outlined in Tables 1 and 2, measurements (b−i). Spectral measurements were done shortly after mixing (Figure 2b−e), and after four months aging in the dark (Figure 3f−i). Each sample is a one-part dilution of stock Si-np in 2-propanol with three-parts of (b, f) 2-propanol,

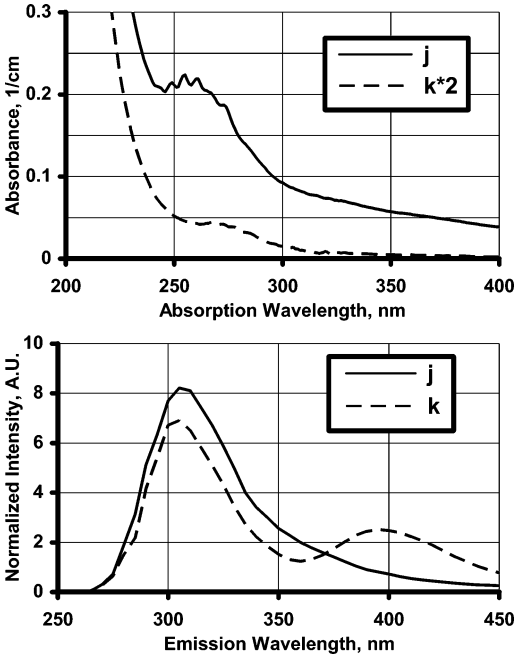

Figure 4. HCl treatment (samples j−k). Samples are: (j) Si-np, already aged four months, prior to treatment, and (k) Si-np after HCl treatment. (Top) Total OD (absorption + scattering). Absorbance of sample (k) is multiplied by two. (Bottom) White-light emission spectra.

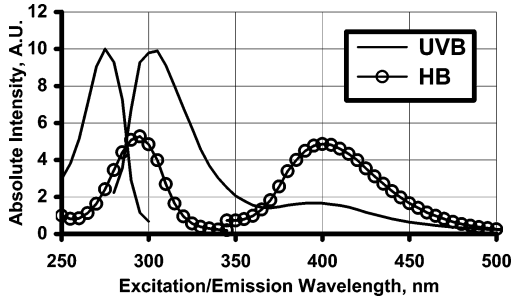

Figure 5. HCl treated sample (k). PL excitation and emission spectra for the UVB (solid) and HB (circles) states. The UVB species has peaks at 275/305 nm (Stokes shift ∼0.45 eV). The HB species has peaks at 295/400 nm (Stokes shift ∼1.1 eV).

(c, g) water, (d, h) NaOH, and (e, i) HCl. The trends in the absorption spectra are consistent with visual observation of the samples. Using the measured OD at 400 nm to quantify the scattering contribution, the order of the freshly mixed samples (Figure 2 and Table 1b−e) with increasing cloudiness is: NaOH (0.4) < 2-propanol (1.0) < water (2.1) < HCl (11.8). After four months aging (Figure 3 and Table 1f−i), the order shifted with: HCl (0.4) ∼ NaOH (0.4) < 2-propanol (1.0) ∼ water (1.3).

We now summarize the overall trends in physical behavior for these samples as a function of time (Tables 1 and 2). The 2-propanol dilution (b, f) had a faint cloudiness, was stable over time with no obvious precipitation, and both the absorption and PL increased in magnitude by ∼50% over four months. Approximately half of this was attributable to solvent evaporation. The water dilution (c, g) was cloudier at first, with the scattering decreasing over time and giving a small amount of precipitation. The absorption and PL both decreased in strength by ∼30% over four months. The NaOH dilution (d, h) was transparent with a large amount of precipitation within hours of preparation. Over four months, the absorption increased slightly and the PL dropped by ∼50%. No further precipitation was observed. The HCl dilution (e, i) was very cloudy at first,

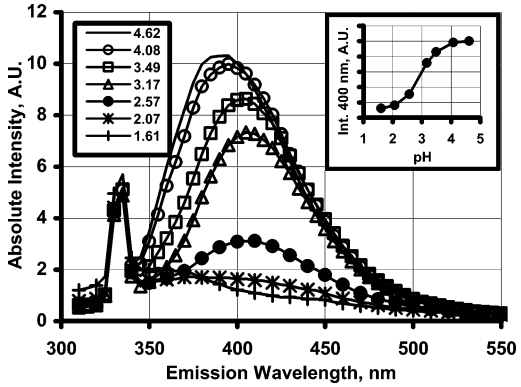

Figure 6. HCl treated sample (k). PL emission spectra for excitation at 300 nm during pH titration. Legend shows pH values. Sharp peak at 330−335 nm is Raman scattering from water. (Inset) Titration curve for PL intensity at 400 nm.

but became transparent over time with precipitation comparable to (d). This occurred at a slower scale of weeks to months and the solids were less compact than those for the NaOH dilution. During the four months of observation, the absorption component decreased slightly, while the PL decreased by ∼75%.

A more detailed view of the PL behavior for the four dilutions is seen by comparing the WES in Figures 2 and 3. Shortly after mixing, the aqueous samples (Figure 2c−e) show a strong red shift in emission from the UV−B state to the UV−A and hard-blue components. The most dramatic change occurred for the NaOH dilution (Table 2d), which showed a large decrease in the UV−B state down to 24%. The PL for this sample is dominated by the UV−A population, with 55% of the total, and there is a smaller increase in the hard-blue emission up to 16%. As summarized in Table 2b−e, the control dilution in water, which has almost identical PL to the HCl dilution, accounts for most of the increase in the hard-blue emission and roughly one-third of the changes in the UV−B and UV−A emissions for the NaOH dilution. The remainder of the redshift from the UV−B to the UV−A population is attributable to the presence of NaOH. Importantly, despite the differing levels of aggregation (scattering) and precipitation discussed above, the overall PL intensity (given as the area under the WES curves) for the fresh dilutions was about the same (± 15%). This suggests that the aggregates are mostly made of dark material and by extension, that the bright material is not as prone to aggregation (see also IV−B, C).

The PL spectra for the NaOH/HCl dilutions after aging four months (Figure 3f−i) show some key changes relative to the fresh dilutions. First, there is a considerable drop in overall intensity for the aqueous samples (Table 2g−i), with the total counts decreasing to 68%, 52%, and 25% of their initial valuesfor the water, NaOH, and HCl dilutions, respectively. The second key difference is in the width of the PL peaks. For the 2-propanol control, the UV−B state is broadened by ∼70 meV after four months, while for the NaOH and HCl dilutions, this state is narrowed by ∼110 meV and ∼50 meV, respectively. The NaOH dilution also has a narrower UV−A population by ∼70 meV. In addition, the Gaussian fit to the WES for the aged NaOH sample (h) is somewhat poor. This is seen most clearly by the sharp rise on the blue-edge of the dominant UV−A peak in Figure 3h. This shows that the narrowing (i.e., quenching) of the PL occurs mostly on the blue-edge. These observations also suggest heterogeneous broadening of the PL (see IV−H).

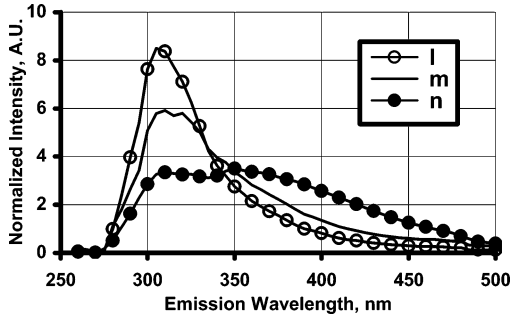

Figure 7. H_2O_2 treatment (samples l−n). White-light emission spectra for: (l) Si-np in 2-propanol, (m) 4× dilution in aqueous H_2O_2, and (n) sample after activation of H_2O_2.

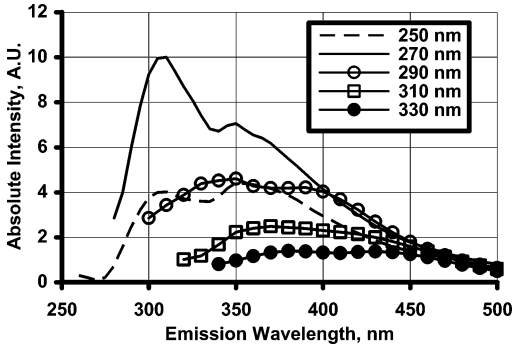

Figure 8. H_2O_2 treated sample (n). PL emission spectra for excitations from 250 to 330 nm.

C. HCl Treatment. Figure 4 and Tables 1 and 2 show two samples for this data set. Sample (j) is the Si-np in 2-propanol, already aged four months, prior to HCl treatment and (k) is the sample redispersed in clean 2-propanol after HCl treatment. There was a substantial loss of material during the two evaporation−redispersion cycles used in this experiment. From the data, it is seen that the Gaussian absorber decreased in magnitude ∼5.3-fold (Figure 4 and Table 1j, k) and the overall PL intensity decreased ∼6.7-fold (Table 2j, k). After HCl treatment, the scattering component followed a $1/\lambda^4$ (Rayleigh) dependence and was negligible in magnitude. Modeling of the WES (Table 2k) shows a decrease in the UV−B and UV−A components, down to 59% and 15% of the total, respectively. This is coupled with a significant increase in the hard-blue population up to 23%. This increase was also seen on an absolute scale when comparing individual emission spectra, demonstrating that there was a net increase in the hard-blue population despite the loss of material.

The individual excitation and emission spectra shown in Figure 5 concentrate on the UV−B and hard-blue emissions after treatment with HCl (sample k). The UV−B state shows the same transitions that were seen in the Si-np stock (Figure 1), with a peak excitation of 275 nm (4.51 eV) and a peak emission of 305 nm (4.07 eV), giving a Stokes shift of 0.44 eV for this state. The transitions for the hard-blue emission are redshifted with the peak excitation at 295 nm (4.20 eV) and the peak emission at 400 nm (3.10 eV), giving a Stokes shift for this state of 1.10 eV. Another relevant quantity for comparison to theory is the PL onset (comparable to the optical gap from theoretical calculations), given as the wavelength (or energy) at which significant PL excitation begins on the red-edge. From the excitation spectra in Figure 5, it is seen that the PL onset for the UV−B and hard-blue populations is ∼300 nm (4.1 eV) and ∼325 nm (3.8 eV), respectively. This is consistent with the absorption modeling (Figure 4 and Table 1j, k) where, after HCl treatment, the Gaussian absorber is red shifted and slightly broadened.

The PL from the hard-blue population was seen to be highly sensitive to pH, with complete quenching of this state at more acidic conditions. Figure 6 shows a series of emission spectra, for excitation at 300 nm, measured during pH titration of the HCl treated Si-np (sample k). The inset shows the titration curve for the relative PL intensity at 400 nm. This simple curve is reminiscent of a single protonation effect, having a pK_a ∼2.9 and a relatively sharp transition with an effective range of pH ∼2.0 to 4.0. There is also an unexplained blueshift in PL of ∼15 nm as the pH is raised, with some hint of another state emerging at higher pK_a on the blue-edge ∼370−380 nm.

D. H_2O_2 Treatment. For comparison, three measurements on the same material under different conditions are included in this data set, as outlined in Tables 1 and 2, samples (l−n). Sample (l) is the stock Si-np in 2-propanol, (m) is a dilution of the stock with three-parts aqueous H_2O_2, and (n) is the same sample after activation of the H_2O_2. The WES for these samples are shown in Figure 7 (l−n). The data for the Si-np in 2-propanol (sample l) are in excellent agreement with the other measurements done on the fresh stock (Table 2a, b, l). The dilution in aqueous H_2O_2 (sample m) is nearly identical to the control dilution in water discussed above (Table 2c, m). And the WES after activation of the peroxide (sample n) shows a roughly equal distribution of the total emission across the UV−B, UV−A, and hard-blue components at 35%, 32%, and 24% of the total, respectively (Table 2n). Also, the blue emission has its largest value of 9.4% for this sample.

Shown in Figure 8 is a series of emission spectra for the H_2O_2 treated Si-np (sample n) with the excitations ranging from 250 to 330 nm. For excitations of 250−270 nm, the UV−B state is well-defined with the peak emission at 305−310 nm. There is also a smaller peak ∼350 nm, which is red shifted 10−15 nm relative to the dominant UV−A emission discussed above for the NaOH dilution. For excitations of 290−330 nm, the PL spectra are not as clearly defined, with two somewhat broadened peaks that red shift with the excitation. The H_2O_2 treatment (n) was the only measurement for which significant emissions were excitable up to ∼330−340 nm. For example, compare these spectra to the emission spectra in Figure 1 (sample a) and the excitation spectra in Figures 9 and 10 (samples j and k, respectively), which cut off for excitations greater than ∼300−320 nm.

IV. Discussion

Here, we discuss the spectral behavior and visual observations for the silicon nanoparticles (Si-np) in 2-propanol and during treatments with water, NaOH, HCl, and H_2O_2, interpreting the results in terms of sample heterogeneity and surface oxidation. First, the preparation method and stock material are discussed and the population of Si-np is coarsely divided into two classes of species, one bright and the other dark. The next two sections focus on the dark material, its fingerprint in the transmission spectra, and its relation to the aggregation and precipitation seen in the NaOH/HCl dilutions. A hydrolysis−condensation mechanism is offered as a reasonable explanation for the observed phenomena. Then, the bright class of material is detailed in several sections focusing on the possible chemical origins of the three distinct PL states observed. The UVB state (UV−B em. ∼305 nm) is correlated with H-passivated Si-np, while the UVA state (UV−A em. ∼340 nm) and the HB state (hard-blue em. ∼400 nm) are correlated with oxide structures on the Si-np surface (Table 4). The final sections summarize the main

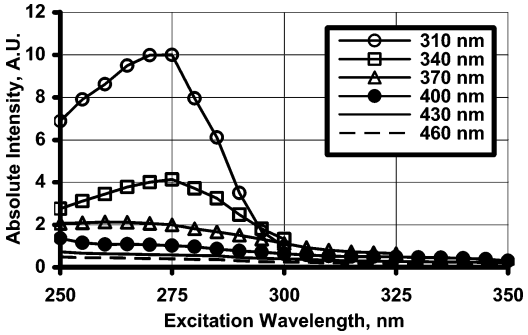

Figure 9. Si-np prior to HCl treatment (sample j). PL excitation spectra for emissions from 310 to 460 nm.

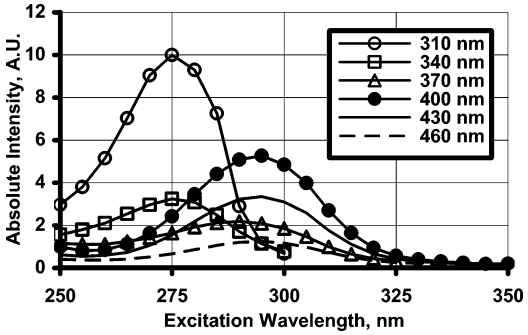

Figure 10. Si-np after HCl treatment (sample k). PL excitation spectra for emissions from 310 to 460 nm.

points and look at the suggested links between sample heterogeneity and spectral broadening.

A. Bright and Dark Material. We begin with a discussion of the preparation method and outline some possible sources for the bright and dark species observed in this work. Preparation of the Si-np starts with anodization of a clean Si wafer using HF and H_2O_2 to etch a porous layer on the surface. Molecular silanes such as $SiF_x(OH)_y$ are continuously produced as the Si atoms are extracted from the wafer during the etching process. These species will be largely removed from the sample since they have good mobility through the porous network and will tend to diffuse into the etchant. They are further diminished with a brief wash between etching and ultrasonication.

The silicon clusters etched from the wafer that are larger than molecular scale, however, diffuse less freely and may become trapped within the pores. Ultrasonic fractionation then crumbles off the porous layer and releases the trapped Si-np into the solvent. The macroscopic fragments of the Si skeleton that break free from the wafer precipitate and are removed from the sample with centrifugation. The Si-np that remain stable in solution, with populations including ultrasmall structures on the 1−3 nm scale, have been observed in previous work on similar samples using TEM imaging and size exclusion chromatography.[10−11]

For the remainder of the discussion, the population of Si-np that are stable in the initial solution (2-propanol) is coarsely divided into two classes of material, one bright and the other dark. The bright material will be shown to have strong PL in the near-UV to blue with a well-defined absorption peak (or shoulder) ∼270 nm. In IV-D, it will be suggested that the average bright species is something similar to the $Si_{29}H_{24}$ cluster (see Figure 11), which is ∼1 nm in diameter and has a monohydride surface passivation. Presumably, this "perfect" cluster is kinetically stabilized against further etching due to the high curvature of its reconstructed surface (see also IV-C).

The dark material will cover a much broader group of Si structures that tend to be unstable against oxidation and aggregation and have relatively weak PL. This includes any molecular silanes that may remain in the sample, partially etched structures that are significantly larger or irregularly shaped, aggregates and chainlike assemblies of many clusters, and nanoscale fragments of the porous skeleton that break free from the Si wafer but remain stable in solution. Large, irregular structures such as these, with overall dimensions of several nm or more, were seen for similar preparations in the TEM imaging of ref 11. They were attributed to aggregates of large numbers of ultrasmall Si-np upon deposition on the graphite grid, but it is also possible that these irregular structures are present in the solution a priori. This type of structure would then be consistent with the dark population outlined here.

B. Dark Material Stability. The presence and behavior of the dark material is seen through its aggregation, scattering, and precipitation in the NaOH/HCl dilutions (Tables 1 and 2, Figures 2 and 3, measurements b−i). The samples in this data set are a one-part dilution of stock Si-np in 2-propanol with three-parts of: (b, f) 2-propanol, (c, g) water, (d, h) NaOH, pH 11.6, and (e, i) HCl, pH 2.2. Visual observation and spectral measurements were taken over a four month period for these samples.

For the fresh dilutions (b−e), the magnitudes of the absorption and total PL were comparable for all of the samples (Tables 1 and 2). Thus, despite the wide variation in cloudiness and aggregation, including the substantial precipitation of material in the NaOH dilution, the overall PL yields were about the same. This strongly suggests that the Si structures that are aggregating tend to be dark. Furthermore, it is seen that the treatment with NaOH is an effective means of removing these dark species from the sample very quickly (within hours), though there is a sizable red shift in the emission from bright species at the same time (see V-E). The HCl dilution (e, i) was also seen to remove dark material, but at a much slower rate of weeks to months. The HCl treatment (sample k) removed dark species, as well, with the two evaporation-redispersion cycles used likely playing a significant role.

Over the four months of observation, the 2-propanol (b, f) and water (c, g) dilutions showed approximately the same overall PL efficiency, with their absorption and PL changing by similar amounts. For the NaOH (d, h) and HCl (e, i) dilutions, however, there is a substantial decrease in overall PL efficiency (i.e., there is a larger decrease in total PL relative to the change in absorption). This suggests that over long times, some fraction of the bright material is darkened through chemical reactions that create defects on the particles, which is consistent with the greater reactivity and harshness of the moderately strong NaOH and HCl dilutions. This also shows that the HCl dilution is not a good route for removal of dark material, since over the long times required, some of the bright species would also be destroyed.

After the samples were aged for four months, the widths of the Gaussian absorber narrowed for all four samples with the fwhm decreasing by ∼10 to 20% (Table 1b−i). This preference for removal or conversion of off-peak absorbers suggests the possibility of a gradual loss of defective structures over time. This notion is further supported by the general observation that the PL excitation spectra have considerably narrower peaks than the Gaussian absorbers.

C. Hydrolysis−Condensation Mechanism. There are many mechanisms that may play a role in the aggregation and precipitation behavior of the NaOH/HCl dilutions. Among these are hydrophobic interactions between H-passivated surfaces, hydrogen-bonding between Si−OH surface groups, hydrogen abstraction ($Si-H + HCl \rightarrow Si-Cl + H_2$) and hydrolysis (Si−

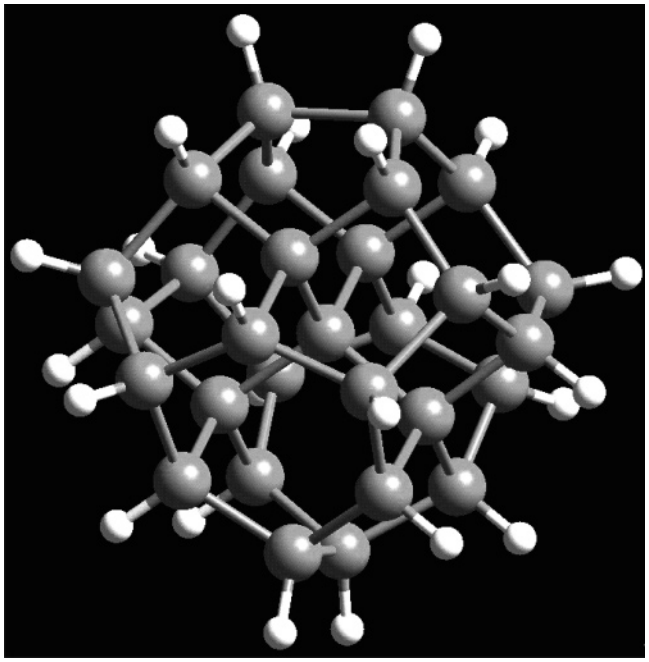

Figure 11. Structural prototype of the $Si_{29}H_{24}$ nanoparticle from ref 10. The Si atoms (gray spheres) are distributed with five forming a tetrahedral core and 24 forming a reconstructed surface passivated with H atoms (white spheres). The nanoparticle is ~1 nm in diameter.

TABLE 3: UVB State Comparison to Theory

Si cluster	Stokes shift	optical gap
$Si_{29}H_{24}$[a]	0.4 eV	3.6 eV
UVB state[b]	0.44 eV	4.1 eV
$Si_{29}H_{36}$[a]	1.0 eV	5.1 eV

[a] Values from ref 22. [b] Peak-to-peak Stokes shift and PL onset.

TABLE 4: Summary of Distinct PL States

state	λ_{ex}	λ_{em}	possible sources	preparation method
UVB	~275 nm	~305 nm	H-passivated hydroxy/alkoxy	stock in 2-propanol
UVA	~275 nm	~340 nm	siloxane-based Si−O−Si bridges	NaOH dilution
HB	~295 nm	~400 nm	silanone-based Si═O group	HCl treatment

Cl + H_2O → Si−OH + HCl), hydrolysis of alkoxy groups (Si−OR → Si−OH), dehydration of silanol groups to form bridge or aggregate structures (Si−OH + HO−Si → Si−O−Si + H_2O), and the formation of silanone-based (>Si═O) structures. This system is particularly complicated since many of these reactions are interdependent and their relative rates will largely depend on the nature of the underlying Si structure (e.g., monohydride versus dihydride oxidation rates).

Nonetheless, the observed aggregation behavior of the dark material may be understood as arising from a simplified two-step, hydrolysis−condensation mechanism. In the first step, the Si structure is oxidized in one of many possible ways, ultimately leading to the formation of Si−OH groups on the surface. The silanol groups then interact through H-bonding pairs to form multiparticle, noncovalent aggregates, which presumably are the source of the strong scattering. For example, NaOH and HCl (and to a lesser extent, water) will enhance the hydrolysis of any alkoxy groups present. The HCl can further catalyze silanol formation through the hydrogen abstraction and hydrolysis mechanism shown above, consistent with the much stronger scattering seen for the HCl dilution shortly after preparation (Figure 2e).

In the second step, neighboring Si−OH groups interacting through H-bonds undergo a dehydration reaction to establish a direct Si−O−Si linkage or bridge structure. The covalent, multiparticle aggregates formed would continue to coalesce and eventually fall out of solution (polycondensation), accounting for the precipitates seen in the samples. Precipitation occurred within hours for the NaOH dilution, while it was considerably slower, occurring over weeks, for the HCl dilution. Also, the solids in the HCl dilution were less compact or more "stringy" than those in the NaOH dilution. These general observations are strongly supported by the results of similar hydrolysis−condensation reactions studied in silicone polymer chemistry and the sol−gel process.[37,38] For example, in ref 37, the author discusses the polycondensation of $Si(OR)_4$ molecules and describes the structure of the products as a "cross-linked spaghetti" for acidic catalysis and a "network of dense particles" for basic catalysis.

Importantly, it was also generally observed that the bright material does not aggregate and precipitate near as much as the dark material. There are several possible explanations for this. First, similar to its resistance to further etching, the bright material may be kinetically stabilized against oxidation and aggregation in solution. This could result from the combination of high surface curvature on the $Si_{29}H_{24}$ cluster (see Figure 11) and the lower reactivity of the monohydride surface. Second, the partially etched and irregular surfaces of the dark material are more likely to contain alkoxy impurities and dihydride and trihydride structures. Thus, they are expected to be more heavily oxidized to start and more easily oxidized after preparation. Third, due to their high surface curvature, it would also be more difficult for two bright particles to form multiple H-bonding pairs simultaneously, which likely helps to stabilize the dark material during the polycondensation step. Finally, the selective removal of the more reactive dark species initially would decrease the overall concentrations of material and further limit the aggregation of bright species at later times.

D. UVB State (Si-np Stock). The UVB state (~305 nm) was most distinct in the measurements on the fresh Si-np stock in 2-propanol (Table 2a, b, l and Figures 1, 2b, and 7l). Previous analysis on similar samples has suggested that the dominant PL source in fresh preparations is a monohydride-passivated species, ~1 nm in diameter.[10−11,21] This is strongly supported by comparisons with the computational modeling of ultrasmall Si clusters done recently by several groups.[22−24] Shown in Table 3 is a comparison with the quantum Monte Carlo simulations of Puzder et al. on the ~1 nm clusters $Si_{29}H_{24}$ (monohydride, reconstructed) and $Si_{29}H_{36}$ (equal mix of monohydride and dihydride passivation).[22] The reported values for the optical gap and Stokes shift for these clusters are compared to the PL onset and peak-to-peak Stokes shift for the UVB state (see Figure 5 and III-C). The observed values of 0.44 eV for the Stokes shift and 4.1 eV for the PL onset are in good agreement with the data for the $Si_{29}H_{24}$ cluster (Table 3), suggesting something similar to this as the average bright species in the Si-np stock.

A likely heterogeneity in the fresh preparation is some amount of surface oxidation, as was observed in previous FTIR measurements.[11] These could arise from myriad sources including incomplete etching and reactions with 2-propanol, water, or trace oxygen during ultrasonication. Among the many types of possible oxidation, as was discussed in ref 22, simple single-bonded oxide species such as hydroxy and alkoxy groups should have relatively minor effects on the PL energies of the Si clusters. Thus, these types of simple oxides should be considered as part of the UVB population. Hydroxy and alkoxy impurities

are also a potential starting point for the slightly more complex oxide structures discussed in the next sections as the possible origins of the UVA and HB populations.

E. UVA State (NaOH Dilution). The UVA state (~340 nm) was most distinct after the dilution of the Si-np stock in 2-propanol with aqueous NaOH (Table 2d, h and Figures 2d and 3h). There are several important details seen in the spectral modeling for this sample. The Gaussian absorber was ~30−40% broader than for the 2-propanol (b, f), water (c, g), and HCl (e, i) dilutions, all of which had about the same width (Table 1). The PL spectra, however, showed about the same widths for all the fresh samples (b−e). The UVA excitation spectrum was very similar to that for the UVB population (peak ~275 nm), while the emission was further red shifted to give a Stokes shift around 0.9 eV. Furthermore, since the UVA state becomes the dominant population after NaOH treatment, whatever the source for this shift is, it should be common to roughly half or more of the bright species.

Simultaneous to the red shift in PL, the dilution in NaOH caused rapid precipitation of the dark material on the scale of hours or less. As was discussed in IV-C, a hydrolysis−condensation mechanism provides a reasonable explanation for this behavior. This suggests siloxane-based structures such as Si−O−Si bridges as a possible origin for the UVA population. These structures could be formed in two steps, both enhanced by the presence of NaOH. First, the coverage of Si−OH groups on the surface of the clusters increases, either through hydrolysis of existing alkoxy impurities or possibly through direct reaction with the hydride. Then neighboring silanol groups dehydrate to form the Si−O−Si bridge or aggregate structure.

Among the many siloxane-based species to consider as possible sources of the UVA population, three candidates will now be discussed. The first is a two-cluster aggregate consisting of two Si particles covalently linked through an oxygen atom. This seems unlikely, however, because the electronic communication between the constituent cores should be very strong and a significant red shift in PL excitation seems likely, but was not observed. Also, with the many potential reactive sites on the surface of a 1 nm Si cluster (roughly 24 or more), there is no reason for the aggregation of bright material, if it was occurring, to be so prominent and yet stop at only two cores. However, there is no indication even after four months aging that higher-order aggregates of bright species are formed in substantial quantities. For example, no substantial red shifts in PL are observed, and the magnitude of the absorption remains roughly constant, actually narrowing over time. All of these are contrary to the usual signs of aggregation.

Another class of siloxane-based structures to consider for the origin of the UVA state is that which can be formed on the surface of a single particle. The possible structures and their relative stability and properties will depend largely on the underlying framework of the Si core (e.g., by requiring different geometries, and hence strains, for the Si−O−Si bond). Thus, models starting from the $Si_{29}H_{24}$ (monohydride) cluster should give distinct results from those starting from the $Si_{29}H_{36}$ (mixed mono/dihydride) cluster. The latter has already been explored computationally in some detail by several groups,[22−24] showing that a stable Si−O−Si bridge can form between next-nearest neighboring dihydride Si atoms (giving the $Si_{29}H_{34}O$ cluster). However, as discussed in the previous section, the data suggests that we are working with something closer to the $Si_{29}H_{24}$, monohydride cluster. Thus, forming a dihydride Si−O−Si bridge would require either breakage of a Si−Si bond, which is unlikely under these conditions, or the presence of some dihydride Si passivation in the initial bright population.

The final candidate offered as a possible source for the UVA state is a monohydride Si−O−Si bridge, which would start from the $Si_{29}H_{24}$ cluster. It could be formed by dehydration of silanol groups between next-nearest neighbors that are connected through an interior Si atom. In looking at the geometric model of the $Si_{29}H_{24}$ cluster in Figure 11, it does appear that such a structure is at least feasible, though it would contain a four-membered ring with considerable strain. More direct physical measurements, along with further computational work starting from the monohydride cluster, some of the permutations between that and the $Si_{29}H_{36}$ cluster, and multicore aggregates linked through a Si−O−Si bridge, should help to decide between these and other possible candidates for the UVA population. The relevant numbers from our data on the UVA state give a PL onset of ~4 eV (small to no change from the UVB state) and a Stokes shift ~0.9 eV (about twice as large as that for the UVB state).

F. HB State (HCl Treatment). The HB state (~400 nm) was most distinct after the HCl treatment (Table 2k and Figures 4k, 5, 6, and 10). Here, we discuss several arguments in favor (and some points against) possible assignment of this state to a silanone-based (>Si═O) structure on the Si-np surface. In an extensive series of investigations, Gole, Dixon, and co-workers[48−56] have correlated the PL from porous Si with emissions from silanone-based silicon oxyhydrides, Si(O)OR, and related structures on the surfaces of the porous network. They also observed that for treatments with moderate to strong HCl, there was a substantial enhancement and subsequent stabilization of this PL.[48−50]

In the simulations of Puzder et al.[22] and Vasiliev et al.,[24] studying H-passivated Si clusters with diameters of 1−2 nm and a single silanone group on their surface, a strong localization of the electronic transitions to the Si═O double bond was demonstrated. A surface state PL mechanism such as this would be consistent with the solvent sensitivity shown by the pH dependence of the hard-blue emission after the HCl treatment (Figure 6). The HB population is completely quenched at pH < 2 and reaches a steady intensity for pH > 4. The titration curve (inset to Figure 6) has a pK_a ~2.9 with a relatively sharp, sigmoidal shape reminiscent of a simple protonation effect. This may be explainable as the equilibrium between a hydrated silanone bond, Si═O·(H_2O), and the hydroxylated surface species, $Si(OH)_2$. As was discussed in IV-D, the latter should be considered as a part of the UVB population. Consistent with this, the PL data shows that as the HB state increases in intensity during pH titration, the UVB state simultaneously decreases in magnitude ~20−25%. This supports the notion of a pH dependent equilibrium between these species/emissions. The peak-to-peak Stokes shift for the HB state, 105 nm or 1.1 eV (see Figure 5 and III−C), is also in good agreement with the same calculations of ref 22. While they studied slightly larger, unreconstructed Si clusters, they reported a steady Stokes shift of ~1.1 to 1.3 eV, relatively independent of size, in excellent agreement with the experimental value.

Inconsistently, though, the reported values for the optical gap of silanone-containing clusters are more than one eV lower than the observed PL onset of ~3.8 eV for the HB state (see Figures 5 and 10). In addition, the quantum chemistry calculations done by Zhou and Head [58] and Prendergast et al.[59] for molecular scale clusters of various silicon oxyhydrides demonstrate that for small molecules, the hydrated silanone bond is unstable relative to the hydroxylated species. These apparent discrepancies, how-

ever, are not definitive in ruling out a silanone-based structure as the source of the HB state. In ref 60, the synthesis of "heavy ketones" (including silanones) was reviewed and it is pointed out that they can be kinetically stabilized by taking advantage of bulky constituents. Thus, it may be possible that for a Si═O double bond in which the Si atom has two back-bonds with the core of the nanoparticle, the silanone structure is somehow stabilized. Another possibility is that the proposed equilibrium does not occur in the ground state, for which the stability calculations were done, but rather it occurs during the excited-state lifetime. This would also address the small observed shift in excitation (PL onset) since the absorption could then occur via the hydroxylated species.

Last, we consider the relatively low abundance of the HB population, which has a maximum strength of about one-quarter of the total emission (Table 2k, hard-blue em.). This may be an indication of the underlying distribution of monohydride and dihydride passivation in the Si-np stock, which was discussed in IV-D as being skewed toward the monohydride surface. On the perfect $Si_{29}H_{24}$ cluster (see Figure 11), it is impossible to form a Si═O double bond without first breaking a Si−Si bond. Thus, either the HCl (pH ∼1.6) is active enough to cleave Si−Si bonds or the initial bright material contains some amount of dihydride passivation.

G. H_2O_2 Treatment and Background Luminescence. In this section, we discuss the H_2O_2 treatment and show a potential correlation with the poorly defined PL seen at several points in this report. The PL data for the sample treated with H_2O_2 (Table 2n and Figure 7n) shows a roughly equal distribution of emissions across the UV−B, UV−A, and hard-blue components; this sample also has the strongest blue emission observed. Figure 8 shows a set of PL spectra with the excitations ranging from 250 to 330 nm for the H_2O_2 treatment (n). The UVB state is well-defined, but the UV-A and hard-blue emissions are not so clear, with the peaks somewhat broadened and red shifting with the excitation. The spectra show that substantial PL is seen for excitations up to 330 nm, which was not observed for any of the other samples. Also, the chemical environment upon activation of the H_2O_2, rich in free radicals propagating quickly and with little distinction, is generally conducive to aggregation of particles. All of these elements, in particular the observed red shift in excitation (PL onset) and the broad and diffuse nature of the PL, are consistent with the source of the poorly defined UV-A, hard-blue, and blue emissions being related to aggregates of small numbers of bright Si-np.

This further suggests a potential correlation between the results of the H_2O_2 treatment and the background luminescence seen in the aqueous dilutions (samples c−e and g−i). The distinction between background PL and well-defined states is most obvious for the data on the hard-blue emission summarized in Table 2. In IV-F, it was argued that the distinct HB state was related to a Si═O double bond on the surface of the Si-np. Comparing the relative strengths of the hard-blue emission among the various samples, however, shows that a significant increase also occurs for the aqueous dilutions (Table 2c−e, g−i). This at first seems contradictory since water cannot be expected to significantly enhance silanone formation. The PL spectra show, however, that the well-defined HB state seen after the HCl treatment (k) is distinct from the other hard-blue emissions (a−j, l−m).

First, the peak wavelengths are red shifted ∼15−20 nm for the HCl treatment relative to the other samples, with the former peaked at 401 nm and the latter from 380 to 385 nm (Table 2). Also note that this emission is not quenched at all for the HCl dilution, as would be expected if it had the same chemical origin as the HB state, which was shown to have a strong pH dependence. Second, the structure of the PL spectra is much different for these two groups of data. Figures 9 and 10 compare the PL excitation spectra for the Si-np in 2-propanol before and after HCl treatment. Before treatment (sample j, Figure 9), the spectra are broader with poorly defined transitions for the redder emissions. After HCl treatment (sample k, Figure 10), the spectra are much sharper and smoother with two well-defined transitions at 275 and 295 nm, respectively. The peak at 295 nm is associated with the HB state (∼400 nm) and was not seen clearly in the spectra prior to treatment.

Finally, differences are also apparent when comparing the PL emission spectra. After the HCl treatment (Figures 5 and 6, sample k), the spectra show a well-defined HB state with smooth spectra and a clear peak ∼400 nm. Whereas for the untreated Si-np in 2-propanol (Figure 1, sample a), the emission spectra have poorly defined transitions for the UV-A, hard-blue, and blue emissions, with no distinct features for PL of 335 nm or greater. Thus, it appears that most of the hard-blue and blue emissions and some of the UV−A emission in the 2-propanol and aqueous dilutions (a−j, l−m) is better attributed to a broad, diffuse background luminescence. The increase in the hard-blue and blue PL for the aqueous dilutions (c−e) and over time (g−i) suggests a possible correlation with aggregation of small numbers of Si-np, similar to that described for the H_2O_2 treatment.

H. Summary (Sample Heterogeneity). We now summarize the main results and attempt to correlate the observed absorption and PL behavior with the various types of heterogeneity discussed. We began with a separation of the Si-np stock into bright and dark material. The dark material was argued to consist of partially etched clusters and fragments, generally larger and more prone to oxidation. The dark species are seen in the NaOH/HCl dilutions with a visible cloudiness and strong scattering for the 2-propanol and water controls, and a substantial precipitation of material in the NaOH and HCl dilutions. To account for the strong scattering, the soft aggregates (noncovalent H-bonding networks) must form scattering centers on the scale of hundreds of nm to microns. Precipitation then likely occurs through polycondensation of this network. The solids formed were clearly visible as a small number of millimeter scale structures, suggesting a sizable mass of dark material on the order of mg/mL. The dark species were also removed by the separate HCl treatment, with the evaporation-redispersion cycles likely enhancing the dehydration of interacting silanol groups.

The bright material was argued to consist of well-etched Si clusters, ∼1 nm in diameter, with a largely monohydride, reconstructed surface that provides some stability versus oxidation and aggregation. The bright species were correlated with the Gaussian absorber peaked at ∼270 nm, accounting for the strong shoulder in the absorption spectra. It is difficult to judge the amount of material present, but given a scatter-corrected absorbance of ∼0.1 cm^{-1} (Figure 1), assuming a rough extinction of $\sim 10^4$ $M^{-1}cm^{-1}$, and using the $Si_{29}H_{24}$ cluster as the basic unit, one can estimate on the order of 10 μg/mL of bright material. To put this mass estimate into perspective, if the average dark particle was 10 times more massive, perhaps an aggregate of 10 bright particles or a partially etched fragment a couple of nm across, then their relative concentrations would be 10 dark particles for every bright particle.

The bright population was then further subdivided into three distinct emitting species (Table 4) referred to as the UVB (∼305

nm), UVA (~340 nm), and HB (~400 nm) states. The UVB population is dominant for the Si-np in 2-propanol (Table 2a, b, f, j, l) and likely consists of H-passivated structures similar to the $Si_{29}H_{24}$ cluster with some minor defects likely. The UVA state was dominant for the NaOH dilution (Table 2d, h) and may originate from siloxane-based structures with Si−O−Si bridges on their surface. The HB population was seen clearly after the HCl treatment (Table 2k), showed a strong pH dependence (Figure 6), and may originate from silanone-based structures with a Si═O double bond on the surface of the nanoparticle.

Within each of these distinct states, there is another level of heterogeneity seen in both the PL and absorption spectra. Focusing first on the PL, Table 2 shows that for all of the fresh samples (a−e and l−n), the UV−B, UV−A, and hard-blue emissions have about the same width (fwhm ~0.47 eV). However, clear signs of heterogeneous broadening are seen in the PL behavior of the NaOH/HCl dilutions over time. After four months aging, there were significant changes in the spectral widths for the 2-propanol, NaOH, and HCl dilutions (Table 2f, h, i). The most dramatic change occurred for the NaOH dilution, which showed a narrowing of both the UV−B and UV−A emissions of ~15−25%. The Gaussian fit to the PL for this sample was somewhat poor and, as seen by comparing Figures 2d and 3h, the narrowing of the dominant UV-A emission occurs on the blue-edge.

Heterogeneous broadening is also seen in the modeling of the absorption spectra (Table 1). The Gaussian absorber was in general ~50−100% broader than the PL states, suggesting that off-peak absorbers tend to be defective, giving them weak PL. For the four samples in the NaOH/HCl dilutions (b−e), the width of the absorption peak decreased by ~10−20% after four months aging (f−i), suggesting a gradual loss or conversion of off-peak absorbers. Also, the absorption broadening (i.e., quenching) is more substantial on the blue-edge, with the PL excitation slightly red-shifted relative to the absorption peaks. Thus, if one of the sources of broadening is population heterogeneities, as appears to be the case, those chemical changes or defects which lead to higher energy transitions also tend to darken the clusters.

This latter observation generally argues against oxidation, already offered as the likely origin of the distinct PL states, as being the common source of PL spectral broadening. The reason being that, for most systems, oxidation is associated with red shifts and, if anything, tends to be destructive to the PL, whereas the quenching seen in this work was toward the blue. One attractive alternative is differences in the abundance of monohydride and dihydride passivation in the starting Si-np preparation. As seen in the modeling of the $Si_{29}H_{24}$ and $Si_{29}H_{36}$ clusters, the latter is of higher energy and can be created from the former by breaking six Si−Si bonds on the surface and adding 12 H atoms. It is also generally true that the dihydride Si structures thus created would tend to be more prone to oxidation and other potentially destructive reactions, establishing a possible link between blue shifts, quenching, and dihydride Si structures on the nanoparticle surface.

V. Conclusions

Experimental and computational work with ultrasmall (few nm or less) silicon nanoparticles (Si-np) is demonstrating the fundamental importance of surface chemistry in dictating their photophysical behavior. For this system, there seems to be considerable opportunity for bridging the gaps between the strengths of organic fluorophores (e.g., small sizes and diverse properties) and the strengths of semiconductor nanoparticles (e.g., narrow, symmetric emissions and good photostability). Many aspects of this potential were seen for the Si-np preparation studied in this work.

Tunability of the photoluminescence was demonstrated with the distinct emissions in the UV−B, UV−A, and hard-blue regions of the spectrum, along with some simple chemical treatments for preparing the different species (Table 4). Further improvement of these and other treatments should provide more quantitative production of the various species, allowing more detailed studies of their physical structures (e.g., by FTIR and NMR) and PL properties (e.g., with UV microscopy). Importantly, larger red shifts in the excitation and emission wavelengths, using slightly larger core sizes if necessary, will also be critical to any widespread use of Si-np in biological systems. For the hard-blue emission (HB state), argued to originate from a silanone-based structure on the surface of the Si-np, measurement of the PL lifetime should provide critical information on whether this emission occurs from a triplet or singlet state. Alternatively, Brandt and Stutzmann have used optically detected magnetic resonance to establish that the red emission from porous silicon occurs from a triplet state.[61]

The pH dependence of the hard-blue emission after HCl treatment shows an exploitable sensitivity to the solvent, consistent with a surface state PL mechanism and signaling some potential for application of Si-np as environmental probes. This is in contrast to compound quantum dots such as CdSe−ZnS−silane nanoparticles, for which the PL originating from the core is largely decoupled from the environment through several layers of required shielding. Nonetheless, this type of multilayered preparation has many inherent benefits and is available to Si-np as well.

Finally, the stability of the H-passivated Si surface versus oxidation and aggregation was discussed in conjunction with the sample heterogeneity. It was seen that the preparation of Si-np through ultrasonic dispersion of bulk Si yields a heterogeneous product that requires further purification to isolate the bright material. Toward this end, it was shown that the bright Si-np were in general more stable, providing routes for their separation from the dark material. The addition of post-preparation treatments, perhaps using a light etch in solution after ultrasonic fractionation, may increase the yield and homogeneity of bright species by recovering some of the material with minor to moderate defects.

All of these elements contribute to the ultimate goal of developing more robust, multifunctional surface passivations for Si-np to be applied as luminescent markers in biological applications. Such efforts, being pursued by many laboratories, seek to combine tunability of the PL properties, the capability for subsequent functionalization, and good stability in aqueous environments, all while maintaining as small an overall size as possible. Progress in these areas is greatly enhanced with the insights coming from computational modeling and through exploitation of the vast knowledge of Si surface and molecular chemistries.

Acknowledgment. The authors thank Dr. M. Nayfeh for providing the Si material for this study. We are also thankful for support from: NIH Institutional NRSA in Molecular Biophysics (5T32GM08276), NIH grant PHS 5 P41−RRO3155, and the University of Illinois at Urbana-Champaign.

References and Notes

(1) Zou, J.; Baldwin, R. K.; Pettigrew, K. A.; Kauzlarich, S. M. *Nano Lett.* **2004**, *4*, 1181.

(2) Yang, C.; Kauzlarich, S. M.; Wang, Y. C. *Chem. Mater.* **1999**, *11*, 3666.
(3) Pettigrew, K. A.; Liu, Q.; Power, P. P.; Kauzlarich, S. M. *Chem. Mater.* **2003**, *15*, 4005.
(4) Mayeri, D.; Phillips, B. L.; Augustine, M. P.; Kauzlarich, S. M. *Chem. Mater.* **2001**, *13*, 765.
(5) Wang, L.; Reipa, V.; Blasic, J. *Bioconjugate Chem.* **2004**, *15*, 409.
(6) Li, Z. F.; Ruckenstein, E. *Nano Lett.* **2004**, *4*, 1463.
(7) Rogozhina, E. V.; Eckhoff, D. A.; Gratton, E.; Braun, P. V. submitted to *J. Mater. Chem.*
(8) Taylor, B. R.; Kauzlarich, S. M.; Delgado, G. R.; Lee, H. W. H. *Chem. Mater.* **1999**, *11*, 2493.
(9) Taylor, B. R.; Fox, G. A.; Hope-Weeks, L. J.; Maxwell, R. S.; Kauzlarich, S. M.; Lee, H. W. H. *Mater. Sci. Eng. B* **2002**, *96*, 90.
(10) Belomoin, G.; Therrien, J.; Smith, A.; Rao, S.; Twesten, R.; Chaieb, S.; Nayfeh, M. H.; Wagner, L.; Mitas, L. *Appl. Phys. Lett.* **2002**, *80*, 841.
(11) Belomoin, G.; Therrien, J.; Nayfeh, M. *Appl. Phys. Lett.* **2000**, *77*, 779.
(12) Akcakir, O.; Therrien, J.; Belomoin, G.; Barry, N.; Muller, J. D.; Gratton, E.; Nayfeh, M. *Appl. Phys. Lett.* **2000**, *76*, 1857.
(13) Nayfeh, M. H.; Barry, N.; Therrien, J.; Akcakir, O.; Gratton, E.; Belomoin, G. *Appl. Phys. Lett.* **2001**, *78*, 1131.
(14) Seto, T.; Kawakami, Y.; Suzuki, N.; Hirasawa, M.; Aya, N. *Nano Lett.* **2001**, *1*, 315.
(15) Patrone, L.; Nelson, D.; Safarov, V. I.; Sentis, M.; Marine, W.; Giorgio, S. *J. Appl. Phys.* **2000**, *87*, 3829.
(16) Holmes, J. D.; Ziegler, K. J.; Doty, R. C.; Pell, L. E.; Johnston, K. P.; Korgel, B. A. *J. Am. Chem. Soc.* **2001**, *123*, 3743.
(17) Lu, X.; Ziegler, K. J.; Ghezelbash, A.; Johnston, K. P.; Korgel, B. A. *Nano Lett.* **2004**, *4*, 969.
(18) English, D. S.; Pell, L. E.; Yu, Z.; Barbara, P. F.; Korgel, B. A. *Nano Lett.* **2002**, *2*, 681.
(19) Nayfeh, M. H.; Rigakis, N.; Yamani, Z. *Phys. Rev. B* **1997**, *56*, 2079.
(20) Allan, G.; Delerue, C.; Lannoo, M. *Phys. Rev. Lett.* **1996**, *76*, 2961.
(21) Mitas, L.; Therrien, J.; Twesten, R.; Belomoin, G.; Nayfeh, M. H. *Appl. Phys. Lett.* **2001**, *78*, 1918.
(22) Puzder, A.; Williamson, A. J.; Grossman, J. C.; Galli, G. *J. Am. Chem. Soc.* **2003**, *125*, 2786.
(23) Puzder, A.; Williamson, A. J.; Grossman, J. C.; Galli, G. *J. Chem. Phys.* **2002**, *117*, 6721.
(24) Vasiliev, I.; Chelikowsky, J. R.; Martin, R. M. *Phys. Rev. B* **2002**, *65*, 1302.
(25) Pizzagalli, L.; Galli, G.; Klepeis, J. E.; Gygi, F. *Phys. Rev. B* **2001**, *63*, 5324.
(26) Eychmüller, A. *J. Phys. Chem. B* **2000**, *104*, 6514.
(27) Michalet, X.; Pinaud, F.; Lacoste, T. D.; Dahan, M.; Bruchez, M. P.; Alivisatos, A. P.; Weiss, S. *Single Mol.* **2001**, *4*, 261.
(28) Gerion, D.; Pinaud, F.; Williams, S. C.; Parak, W. J.; Zanchet, D.; Weiss, S.; Alivisatos, A. P. *J. Phys. Chem. B* **2001**, *105*, 8861.
(29) Bruchez, M., Jr.; Moronne, M.; Gin, P.; Weiss, S.; Alivisatos, A. P. *Science* **1998**, *281*, 2013.
(30) Dubertret, B.; Skourides, P.; Norris, D. J.; Noireaux, V.; Brivanlou, A. H.; Libchaber, A. *Science* **2002**, *298*, 1759.
(31) Chan, W. C. W.; Nie, S. *Science* **1998**, *281*, 2016.
(32) Larson, D. R.; Zipfel, W. R.; Williams, R. M.; Clark, S. W.; Bruchez, M. P.; Wise, F. W.; Webb, W. W. *Science* **2003**, *300*, 1434.
(33) Parak, W. J.; Gerion, D.; Zanchet, D.; Woerz, A. S.; Pellegrino, T.; Micheel, C.; Williams, S. C.; Seitz, M.; Bruehl, R. E.; Bryant, Z.; Bustamante, C.; Bertozzi, C. R.; Alivisatos, A. P. *Chem. Mater.* **2002**, *14*, 2113.
(34) Willard, D. M.; Carillo, L. L.; Jung, J.; Orden, A. V. *Nano Lett.* **2001**, *1*, 469.
(35) Mattoussi, H.; Mauro, J. M.; Goldman, E. R.; Anderson, G. P.; Sundar, V. C.; Mikulec, F. V.; Bawendi, M. G. *J. Am. Chem. Soc.* **2000**, *122*, 12142.
(36) Mayne, A. H.; Bayliss, S. C.; Barr, P.; Tobin, M.; Buckberry, L. D. *Phys. Status Solidi A* **2000**, *182*, 505.
(37) Brook, M. A. *Silicon in Organic, Organometallic, and Polymer Chemistry*; John Wiley & Sons: New York, 2000.
(38) Hench, L. L.; West, J. K. *Chem. Rev.* **1990**, *90*, 33.
(39) Waltenburg, H. N.; Yates, J. T., Jr. *Chem. Rev.* **1995**, *95*, 1589.
(40) Stewart, M. P.; Buriak, J. M. *Comments Inorg. Chem.* **2002**, *23*, 179.
(41) Buriak, J. M. *Chem. Commun.* **1999**, 1051.
(42) Sieval, A. B.; Demirel, A. L.; Nissink, J. W. M.; Linford, M. R.; Maas, J. H.; Jeu, W. H.; Zuilhof, H.; Sudhölter, E. J. R. *Langmuir* **1998**, *14*, 1759.
(43) Buriak, J. M.; Stewart, M. P.; Geders, T. W.; Allen, M. J.; Choi, H. C.; Smith, J.; Raftery, D.; Canham, L. T. *J. Am. Chem. Soc.* **1999**, *121*, 11491.
(44) Li, X. J.; Zhang, Y. H. *Phys. Rev. B* **2000**, *61*, 12605.
(45) Zhang, Y. H.; Li, X. J.; Zheng, L.; Chen, Q. W. *Phys. Rev. Lett.* **1998**, *81*, 1710.
(46) Yu, D. P.; Bai, Z. G.; Wang, J. J.; Zou, Y. H.; Qian, W.; Fu, J. S.; Zhang, H. Z.; Ding, Y.; Xiong, G. C.; You, L. P.; Xu, J.; Feng, S. Q. *Phys. Rev. B* **1999**, *59*, 2498.
(47) Wang, J.; Song, L.; Zou, B.; El-Sayed, M. A. *Phys. Rev. B* **1999**, *59*, 5026.
(48) Gole, J. L.; DeVincentis, J. A.; Seals, L.; Lillehei, P. T.; Prokes, S. M.; Dixon, D. A. *Phys. Rev. B* **2000**, *61*, 5615.
(49) Dudel, F. P.; Gole, J. L. *J. Appl. Phys.* **1997**, *82*, 402.
(50) Seals, L.; Dudel, F.; Grantier, D.; Gole, J. L.; Bottomley, L. A. *J. Phys. Chem. B* **1997**, *101*, 8860.
(51) Gole, J. L.; Dixon, D. A. *J. Phys. Chem. B* **1998**, *102*, 1768.
(52) Gole, J. L.; Dixon, D. A. *Phys. Rev. B* **1998**, *57*, 12002.
(53) Gole, J. L.; Dixon, D. A. *J. Phys. Chem. B* **1998**, *102*, 33.
(54) Gole, J. L.; Dixon, D. A. *J. Phys. Chem. B* **1997**, *101*, 8098.
(55) Gole, J. L.; Dudel, F. P.; Grantier, D.; Dixon, D. A. *Phys. Rev. B* **1997**, *56*, 2137.
(56) Dixon, D. A.; Gole, J. L. *J. Phys. Chem. B* **2005**, *109*, 14835.
(57) Yamani, Z.; Thompson, W. H.; AbuHassan, L.; Nayfeh, M. H. *Appl. Phys. Lett.* **1997**, *70*, 3404.
(58) Zhou, F.; Head, J. D. *J. Phys. Chem. B* **2000**, *104*, 9981.
(59) Prendergast, D.; Grossman, J. C.; Williamson, A. J.; Fattebert, J.; Galli, G. *J. Am. Chem. Soc.* **2004**, *126*, 13827.
(60) Okazaki, R.; Tokitoh, N. *Acc. Chem. Res.* **2000**, *33*, 625.
(61) Brandt, M. S.; Stutzmann, M. *Solid State Commun.* **1995**, *93*, 473.